International Journal of Applied Ceramic Technology
Ceramic Product Development and Commercialization

$10Sc_2O_3{\cdot}1CeO_2{\cdot}89ZrO_2$ as electrolyte for SOFCs. Sintering and ionic conductivity of thin, flat sheets

Journal:	*International Journal of Applied Ceramic Technology*
Manuscript ID	ACT-3921.R1
Manuscript Type:	Article
Date Submitted by the Author:	n/a
Complete List of Authors:	Escardino, Agustin; Universitat Jaume I., Chemical Engineering Department Belda, Adriana; Universitat Jaume I., Chemical Engineering Department Orts, M-Jose; Universitat Jaume I, Chemical Engineering Department Gozalbo, Ana; Universitat Jaume I., Chemical Engineering Department
Keywords:	zirconia, tape casting, conductivity, grain size

$10Sc_2O_3 \cdot 1CeO_2 \cdot 89ZrO_2$ as electrolyte for SOFCs. Sintering and ionic conductivity of thin, flat sheets

Agustín Escardino, Adriana Belda , Maria-Jose Orts, Ana Gozalbo*

Departamento de Ingeniería Química. Instituto Universitario de Tecnología Cerámica. Universitat Jaume I, Castellón, 12006 Spain.

Abstract

Thin, flat sheets, about 90µm thick, were prepared from ceria-doped scandia-stabilized zirconia with formula $10Sc_2O_3 \cdot 1CeO_2 \cdot 89\ ZrO_2$ (hereafter 10Sc1CeSZ) by tape casting and subsequent sintering at different thermal cycles.

A sintering thermal cycle was selected that yielded defect-free flat sheets, with practically negligible porosity (between 0.35 and 0.10%) and average grain diameters ranging from 1.32 to 6.30 µm.

Ionic conductivity at 600°C was as high as 21 mS/cm. Ionic conductivity increased with average grain diameters up to 2.7 µm. At higher average grain diameters, conductivity remained practically constant.

Keywords: Tape casting; Grain size; conductivity; zirconia.

1 Introduction

Zirconia solid solutions with certain oxides of Group IIIB elements have been widely studied in recent years, owing to their possible use as electrolytes in solid oxide fuel cells (SOFCs).

Until the beginning of this century, Y_2O_3-stabilized zirconia was the most widely studied solid solution [1-5]. However, these materials have the drawback that their conductivity progressively

* gosalbo@uji.es

Supported by the European Community within the integrated project SOFC600 (contract no. 020089)

declines [6-7], when they operate in the range of temperatures in which their conductivity has an acceptable value (from 800 to 1000°C) [8,9].

During the last few years, it has been widely sought to improve the ionic conductivity of zirconia solid solutions at progressively lower temperatures to avoid their thermal degradation [10,11]. Sc_2O_3-stabilized zirconia, in its cubic crystalline form, exhibits higher ionic conductivity at intermediate temperatures (700–900°C) than Y_2O_3-doped zirconia [12-14]. Good results have also been obtained when zirconia is doped with Y_2O_3 and Sc_2O_3 [15,16], the results being even better when the dopants are CeO_2 and Sc_2O_3 [17-19].

This study was undertaken to obtain flat defect-free electrolyte sheets, less than 100 μm thick, with a porosity below 5%, and having appropriate mechanical strength and ionic conductivity when operating at temperatures ranging from 600 to 700°C (IT-SOFCs). The study was conducted using ceria-doped scandia-stabilized zirconia with molecular formula $10Sc_2O_3.1CeO_2.89ZrO_2$ (10Sc1CeSZ). Sintered samples of this composition have yielded ionic conductivities of up to 16 mS/cm, operating at 600°C [19].

Flat sheets of the specified thickness were formed by tape casting, this technique being commonly used in industrial practice for manufacturing thin sheets and films of ceramic materials at a relatively low cost. The sheets formed by this method exhibit a smooth surface, precise dimensions and, if the additives are optimized, appropriate dry mechanical strength for handling before sintering [20]. The following components are usually added in tape casting: a liquid for suspending the powder and dissolving the necessary organic additives, a dispersant, a binder [21], plasticizers, and sometimes a homogenizer.

The higher the organic additives content in the dry sheet, the higher the porosity of the sheet after organic matter burnout under non-isothermal conditions. The arising stresses in this stage can lead to dimensional variations, cracking and other microstructural defects in the sheet [22]. Burnout has therefore to be performed at a very low heating rate [23]. The ensuing sintering process is usually conducted in two steps: a first one, under non-isothermal conditions, at a very low rate up to the pre-set sintering temperature and a second one, in which the pieces are isothermally treated at this temperature for a certain time.

2 Experimental Procedure

The 10Sc1CeSZ powder used as basic component came from the Japanese company DKKK (Daiichi Kigenso Kagaku Kogyo Co. Ltd.) and was supplied by the German company Sumitomo Deutschland GmbH. The specific surface of this powder, determined by the BET method, was 11 m^2/g.

The solvents used (methyl ethyl ketone, isopropanol, xylene, and ethanol) were analytical grade reagents. Menhaden fish oil (MFO) was used as dispersant while dibutyl phthalate (DBP) and polyethylene glycol 400 (PEG-400) were used as plasticizers. Polyvinyl butyral (PVB) was chosen as binder.

The electrolyte sheets were formed by tape casting suspensions of 10Sc1CeSZ powder in two different mixtures of solvents: a) methyl ethyl ketone (MEK) and isopropanol and b) xylene and ethanol. The suspensions were homogenized in a FRITSCH Pulverisette 5 planetary mill in two consecutive steps to prevent the competitive adsorption of the dispersant and binder onto the 10Sc1CeSZ particles [21,24]. In the first step, the solvent mixture, dispersant, and the 10Sc1CeSZ powder were milled for six hours. In the second, the plasticizers and binder were added, stirring for sixteen hours. Air was then removed under low pressure, avoiding solvent evaporation. Suspension apparent viscosity was then measured at a temperature of 25°C, in order to relate apparent viscosity to flowability in the tape casting equipment [25,26]. The sheets were tape cast onto a polyethylene film that moved across the doctor-blade table, where they were left to dry for 24 hours before cutting them into pieces of different sizes.

Cylindrical test pieces were obtained by uniaxial pressing of 1g samples of 10Sc1CeSZ with an organic binder, in an Instron Universal Testing Machine, at a pressure of 80 MPa, in a 19 mm-diameter die.

The dry test pieces were heat treated in two consecutive steps. The first step, aimed at burning out the organic matter, was carried out at a constant heating rate. The second step was performed in two stages: a constant heating rate up to sintering temperature followed by a dwell time at that temperature. In the case of the sheets obtained by tape casting, the pieces were placed in a sandwich arrangement between two porous refractory slabs (Repton tiles) during heat treatment.

The DTA-TG was done in a Mettler Toledo TGA/SDTA 851e, under air atmosphere, at a heating rate of 2°C/min up to a temperature of 1400°C.

The sintering curves (variation of shrinkage with temperature) of the dry sheets were determined by hot stage microscopy (HSM) in a MISURA 3 by Expert System Solutions at a heating rate of 2°C/min, in air atmosphere. The hot-stage microscopy (HSM) is the combination of a heating stage (hot stage) with a sample holder coupled with a light microscope and a system that allows to record the changes in shape and geometry of a sample with temperature when submitted to a thermal cycle.

The crystalline phases present in the sintered samples were determined by XRD with a D8 Advance BRUKER diffractometer.

Cross sections of the samples were embedded in an epoxy resin and then polished to 1µm with diamond paste, in order to measure their porosity and grain size.

Porosity was measured by image analysis (Olympus MicroImage v4.0) of SEM images of the polished samples obtained in a FEI QUANTA 200 FEG scanning electron microscope. Total porosity (area %) and pore size distribution were determined for every sample. The characteristic size chosen for the pores was the “projected area diameter” [27], defined as the diameter of the circle having the same area as the pore section, and calculated from the pore section area (A_p) as:

$$d_p = 2\sqrt{\frac{A_p}{\pi}} \qquad \text{(Eq. 1)}$$

The grain size of the sintered specimens was measured from SEM images of thermally etched samples (to reveal grain boundary [28,29]), using the same image analysis software. The grain size for every particle (D_g) was also calculated as the projected area diameter:

$$D_g = 2\sqrt{\frac{A_g}{\pi}} \qquad \text{(Eq. 2)}$$

where A_g was the area of the grain section. The values obtained were classified and weighted in area to obtain the particle size distribution; the average grain size (D_{50}) was taken as the median value of this area-weighted distribution [30-32].

The cylindrical sintered specimens intended for the measurement of the ionic conductivity were coated on both sides with platinum paste to obtain the electrodes. The coated samples were then dried in an oven at 110°C and heat treated in an electric laboratory furnace at 850°C for 60 minutes.

Conductivities were measured by complex impedance spectroscopy [33] with an impedance analyzer Solartron 1260, connected to a tubular furnace with a measurement cell consisting in two contact points and four platinum wires. The measurements were made under atmospheric conditions at 600°C. The frequency was varied between 10^2 Hz and 10^7 Hz. The perturbation applied was 100 mV. Total conductivity, as well as bulk grain and grain boundary conductivities, were determined from the impedance spectra by using the ZView2 software.

The flexural strength of the sintered sheets was measured by the “ball-on-ring” method from biaxial flexure tests [34], performed in an Instron Universal Testing Machine.

The measuring device consisted of a steel support with a central hole, on which the specimen to be tested was located. On this, a load was applied by means of a piston which, in the part in contact with the specimen, was rounded and that was advancing at a constant speed of 1 mm/min. In the test, the breaking force of each sample is determined and the flexural strength is calculated from its value, according to the expression proposed by Shetty [34].

3 Results and discussion

3.1 Preparing the 10Sc1CeSZ suspensions and casting the sheets

Several suspensions were prepared from the 10Sc1CeSZ powder by using two different liquid systems: a) a mixture of methyl ethyl ketone (MEK) with isopropanol and b) a mixture of xylene and ethanol. In both cases, the proportions of liquids and additives (binders, plasticizers and dispersants) were modified in order to find the suspension that, after tape casting, provided sheets with the desired characteristics.

The criteria used to select the optimal conditions were, in the first place, the possibility to produce very flat sheets without defects and secondly, to introduce the lowest possible amount of additives.

A total of 23 suspensions were prepared with the mixture MEK-isopropanol. The composition leading to the best dry films contained (in wt%) 42.8% 10Sc1CeSZ, 25.9% MEK, 16.9% isopropanol, 1.7% MFO, 1.2% DBP, 3.0% PEG-40 and 8.6% PVB. The quality of the sheet obtained casting this suspension was very good. However, the content in organic matter of the dry sheet was too high, around 25 wt%, resulting in an excessive porosity after sintering. With the objective to reduce the amount of organic additives, a new mixture of liquids (xylene-ethanol) was selected to prepare the suspensions.

Using xylene-ethanol as solvent, 18 different suspensions were tried. The best dry and sintered sheets were obtained from a suspension prepared with (weight percent) 59.7% 10Sc1CeSZ, 14.8% of xylene, 14.8% ethanol, 1.8% MFO, 3.6% DBP, 1.2% PEG-400 and 4.2% PVB. The aspect of the cast sheet is shown in Fig. 1.

The use of this last suspension to form the sheets should lead to obtaining sintered samples of better quality. Indeed, increasing the solids content from 43% (using MEK-isopropanol as solvent) to 60% should reduce the shrinkage experimented by the sheets during the drying (solvent removal) step. On the other hand, reducing the content of organic additives (MFO, DBP, PEG-400, PVB), in the dry sheets, from 25 to 15.3%, should reduce the porosity of the samples resulting from the organic matter removal step, prior to sintering. Both circumstances should contribute to obtaining sintered samples with less defects and lower porosity.

3.2 Designing the thermal treatment to remove the organic additives and sinter the dry sheets.

In order to optimize the thermal cycle and obtain sintered sheets without defects (such as cracks, warping or loss of planarity) a DTA-TG and a hot-stage microscopy of the dry composition (the optimal for the MEK-isopropanol mixture) were performed.

The TG diagram obtained (Fig. 2) shows two clearly distinct peaks: one broader, with its maximum at 283°C, and another narrower, with its maximum at 371°C that ends around 450 °C.

The DTA diagram in Fig. 3 confirms the results obtained in the TG essay, for it shows two exothermic peaks that should arise from the combustion of the organic additives. No other

peaks, due to either mass or phase changes, are observed at higher temperatures, which implies that the cubic zirconia undergoes no transformation during the sintering step.

This fact was further confirmed by an XRD analysis of a dry sheet of the same composition, treated for the organics removal and then sintered to 1500°C. When compared with the XRD analysis of the starting zirconia powder, it was assessed that the diffractogram hadn't changed and only those peaks pertaining to the cubic zirconia appeared.

Hot stage microscopy was also carried out in air atmosphere, at a heating rate of 2°C/min and up to 1350°C, for the best dry composition obtained in the system xylene-ethanol. The result is presented in Fig. 4, as linear shrinkage versus temperature. There is a first period of sharp shrinkage due to the organics removal, with a maximum shrinkage rate at about 215°C; then, shrinkage halts at about 420°C and the test piece expands slightly until it reaches 895°C. At this temperature, the sintering stage begins and the sample shrinks again till it reaches 1350°C, maximum temperature of the thermal cycle.

From the results of the previous tests, it can be concluded that the burnout stage of the dry samples (obtained either by tape casting or by pressing), in an air atmosphere and at a heating rate of 2°C/min, ends around 450°C.

To verify this fact, the dry sheets were heated at 2°C/min to different maximum temperatures, ranging from 300 to 600°C. The aspect of some of them after heat treatment is shown in Fig. 5. At 300°C, the sheet was blackish due to the coking of the organic additives, while the sample treated to 400°C was almost white but with a gray shade that implied there was still some carbon left. At 500°C, the removal of the organic additives was complete and the sheet obtained was white. At higher temperatures, though, the samples cracked. None of the sheets obtained in those conditions had the desired planarity, so the heating rate was lowered to 1°C/min and then, even further, to 0.5°C/min.

Fig. 6 shows the sheets obtained at the heating rate of 0.5°C/min to several maximum temperatures. It can be observed that, at this lower heating rate, the removal of the organic material is complete even at 400°C and, at the maximum temperature of 500°C, the sheets are free of defects and retain their original planarity. So, a heating rate of 0.5°C/min and a maximum temperature of 500°C was chosen for the burnout stage of the subsequent samples.

After the burnout, the heating rate to the sintering temperature had to be considered. Different heating rates were tried, finally choosing 2°C/min as the highest one that allowed to obtain sintered sheets free of defects. The peak temperatures chosen for the sintering step ranged from 1200 to 1500°C.

3.3 Sintering the sheets.

After the burnout, the sheets were heated at a heating rate of 2°C/min from 25°C up to four different sintering temperatures (T_S) of 1200, 1300, 1400 and 1500°C, at which they remained in isothermal conditions for 2, 4 or 6 hours. Then, their porosity (ε), mean pore diameter (d_{50}) and average grain size (D_{50}), were measured.

Fig. 7 graphs the porosity (ε) and mean pore diameter (d_{50}) values of the sheets versus their holding time (t_h) at each one of the four sintering temperatures. It can be observed that:

a) The porosity of the sheets sintered at 1300,1400 and 1500°C is quite similar (between 0.35 and 0.10%) and hardly changes with holding time. The lowest values (0.10 - 0.11 %) are those obtained for the sheets sintered at 1400°C (t_h = 6h) and 1500°C (t_h = 4 and 6 h); those specimens can be admitted to be practically free of porosity.

b) The porosity of the sheets sintered at 1200°C during 2 and 4 hours is much higher, reaching values that far exceed the acceptable limits.

c) The pore average diameter is little affected by the holding time and its value ranges between 0.34 and 0.18 μm, at the four sintering temperatures studied. The lowest values are obtained for the sintering temperatures of 1300 and 1400°C.

Fig. 8 shows the SEM images of the grains in the surface of the sheets treated at the four sintering temperatures (T_S) for different holding times (t_h), at the same magnification. It can be seen that though grain size increases both with temperature and holding time, the influence of temperature is much greater than that of the holding time. The evolution of the average grain size of these samples (D_{50}), measured by image analysis, with the holding time at each temperature, is presented in Fig. 9.

3.4 Sintering the cylindrical pressed specimens.

On measuring the ionic conductivity of the sintered sheets, the values obtained were widely scattered and unreliable, very likely because the samples were less than 0.1 mm thick, much

thinner than those usually measured by impedance spectroscopy, that range between 0.8 and 4 mm of thickness [35-37].

Therefore, in order to measure the conductivity, cylindrical specimens, 14mm in diameter and 1.12 mm thick, were uniaxially pressed from a mixture of 10Sc1CeSZ powder and organic binder. The pressed samples were then subjected to the same thermal treatments as the dry sheets.

Nevertheless, before measuring their conductivity, it was considered necessary to assess whether their porosity and grain size were comparable to that of the cast sheets sintered in the same conditions, as both porosity and grain size influence the ionic conductivity.

Fig. 10 shows the evolution of porosity (ε) and mean pore diameter (d_{50}), for the sintered pressed specimens as a function of holding time (t_h), for three sintering temperatures. As can be seen, at the two highest sintering temperatures, porosity is comprised between 0.4 and 1% while for the sheets sintered at the same temperatures, porosity varied from 0.1 to 0.35% (see Fig. 7). As regards the mean pore diameter, it was around 0.3 μm in the sintered pressed specimens, quite similar to that of the sintered sheets.

Fig. 11 shows the evolution of the average grain size of the pressed specimens, both with the sintering temperature (1300, 1400 and 1500°C) and the holding time (1 to 6 hours). As can be seen, the average grain size values are very similar for pressed specimens and sheets at the sintering temperatures of 1300 and 1400°C. Only at the highest sintering temperature, 1500°C, the grain sizes of the sheets (4.75, 5.71 and 6.30 μm) are larger than those of the pressed specimens (3.80, 4.30 and 4.70 μm).

3.5 Ionic conductivity of the sintered pressed specimens.

The ionic conductivity of the sintered pressed specimens was measured at several temperatures, ranging from 300°C to 1000°C. Fig. 12 shows the impedance spectra of these specimens at the test temperatures of 300 and 600°C.

Given that the electrolyte studied must be applicable for intermediate or low-temperature solid oxide fuel cells (SOFCs), Table 1 lists only the values of total ionic conductivity (σ_T) obtained for

the sintered pressed specimens at 600°C. The sintering conditions (T_S and t_h) are also included, as well as the average grain size of the sintered pressed specimens (D_{50PS}).

From the values shown in Table 1, the following is deduced:

a) In the specimens sintered at 1300°C, conductivity increases with the average grain size until it reaches 2.7 μm, while at the two highest sintering temperatures (1400 and 1500°C), conductivity values remain practically constant around an average of 21.5 mS/cm (the fluctuations around that value falling within the experimental error of ±0.5 mS/cm). This result seems to indicate that, for D_{50} larger than 2.7 μm, the increase in grain size no longer affects the total conductivity value. This behaviour has been repeatedly observed throughout all the range of test temperatures studied, between 300 and 1000 °C [42] and agrees with the results obtained by Lee et al. [17].

b) At the sintering temperatures of 1400 and 1500 ºC, the maximum value of the total conductivity in the sintered samples is already reached for holding times of 2 hours.

c) The total ionic conductivities obtained are of the same order but slightly higher than the ones obtained so far, for scandium and cerium doped zirconia electrolytes for SOFC cells at the test temperature of 600°C, by other researchers. Indeed, the reviewed literature reports total conductivity values, at 600°C, that vary from 3 to 15 mS/cm [38–41].

When comparing the grain size of the sintered pressed pellets obtained in this work with that of similar samples obtained by other researchers, no significant differences were found in most cases [38, 39] so it doesn't seem likely that the improvement in conductivity results from a difference in the grain size. Perhaps the reason why the conductivities of the pressed specimens obtained in this work are higher than those of similar samples in the literature is that their porosity, between 0.4 and 1 %, is quite low.

An issue that could arise is the applicability of the values of total ionic conductivity measured in the pressed pellets to the sheets sintered at the same temperature and holding time. Given the little difference existing between the values of the structural properties (ε, d_{50} and D_{50}) of the sheets and of the sintered pressed pellets (Table 2), and taking into account that the conductivity seems to be virtually independent of grain size when it exceeds 2.7 μm, the conductivity of the sheets can be expected to be quite similar to that of the pressed specimens.

In fact, as the porosity of the sintered sheets is lower than that of the pressed specimens, their conductivity could even be slightly higher. Therefore, we consider that the conductivity values measured on the pressed specimens can be accepted as representative of the conductivity of the sheets sintered in the same conditions.

3.6 Fracture strength of the sintered sheets

The fracture strength was measured in 90-µm-thick sheets, sintered at 1400°C during 6 hours, obtaining a value of 121 MPa. The sheets were somewhat fragile, so their thickness should be slightly increased to improve the handling of the specimens.

4 Conclusions

It has been possible to obtain dry flat sheets of 10Sc1CeSZ with a thickness of 90µm, without defects, by tape casting a suspension of the particles in xylene-ethanol and other organic additives (binders, plasticizers and dispersants).

The thermal cycle has been optimized. In a first step, the organic additives contained in the dry sheets have been burnt out in non-isothermal conditions, at a heating rate of 0.5°C/min from room temperature up to 500°C. In a second step, the burnout sheets have been heated at 2°C/min up to the desired sintering temperature, and held at that temperature for different holding times.

The sintered sheets have very low porosity (between 0.35 and 0.10 %) and an average grain size that increases with sintering temperature and holding time from 1.32 to 6.30 µm.

Due to the difficulty of measuring the conductivity in the sintered sheets, cylindrical specimens, 1.12 mm thick, have been prepared by isostatic pressing of a mixture of 10Sc1CeSZ powder and organic additives. The specimens have then been subjected to the same heat treatment than the sheets, both for the burnout and the sintering steps.

The sintered samples have conductivity values, at 600°C, of 21 mS/cm, higher than the values usually reported in the literature, probably due to the high pressures used to form the cylindrical specimens, which have led to sintered samples with very low porosity.

In the operational conditions employed, the conductivity increases with the average grain size until it is around 2.7 μm. For larger grain sizes, conductivity is virtually constant.

References

1. J.B. Goodenough, Oxide-Ion Electrolytes, *Annu. Rev. Mater. Res.,* 33 91-128 (2003).

2. Y.K. Lee, J.W. Park, Microstructure and electrical conductivity of yttria-stabilized zirconia electrolyte thin plates produced by the doctor blade method, *Jour. Mater. Sci. Lett*., 16 678-682 (1997).

3. Y. Arachi, T. Asai, O. Yamamoto, Y. Takeda, N. Imanishi, K. Kawate, C. Tamakoshi, Electrical Conductivity of ZrO_2-Sc_2O_3 Doped with HfO_2, CeO_2, and Ga_2O_3, *Jour. Electrochem. Soc.*, 148 [5] A520-A523 (2001).

4. K. Yamahara, T. Z. Sholklapper, C. P. Jacobson, S. J. Visco, L. C. De Jonghe, Ionic Conductivity of Stabilized Zirconia Networks in composite SOFC Electrodes, *Solid State Ionics*, 176 1359–1364 (2005).

5. K. Chen, Z. Lü, N. Ai, X. Huang, Y. Zhang, X. Xin, R. Zhu, W. Su, Development of yttria-stabilized zirconia thin films via slurry spincoating for intermediate-to-low temperature solid oxide fuel cells, *Jour. Pow. Sour.*, 160 [1] 436-438 (2006).

6. S. P. S. Badwal, Zirconia-based solid electrolytes: microstructure, stability and ionic conductivity, *Solid State Ionics,* 52 [1-3] 23-32 (1992).

7. S. P. S. Badwal, Stability of solid oxide fuel cell components, *Solid State Ionics,* 143 [1] 39-46 (2001).

8. J. M. Dixon, L. D. LaGrange, U. Merten, C. F. Miller, J. T. Porter II, Electrical Resistivity of Stabilized Zirconia at Elevated Temperatures, *J. Electrochem Soc.,* 110 [4] 276-280 (1963).

9. D. W. Strickler, W.G. Carlson, Electrical Conductivity in the ZrO_2-Rich Region of Several M_2O_3—ZrO_2 Systems, *J. Am. Ceram. Soc.,* 48 [6] 286-289 (1965).

10. J.M. Ralph, A.C. Schoeler, M. Krumpelt, Materials for lower temperature solid oxide fuel cells. *Journal of Materials Science*, 36 [5] 1161-1172 (2001).

11. T.I. Politova, J.T.S. Irvine, Investigation of scandia-yttria-zirconia system as an electrolyte material for intermediate temperature fuel cells- influence of yttria content in system $(Y_2O_3)_x(Sc_2O_3)_{(11-x)}(ZrO_2)_{89}$. *Solid State Ionics,* 168 [1-2] 153-165 (2004).

12. M. Hirano, M. Inagaki, Y. Mizutani, K. Nomura, M. Kawai, Y. Nakamura, Mechanical and electrical properties of Sc_2O_3-doped zirconia ceramics improved by postsintering with HIP, *Solid State Ionics*,133 [1-2] 1-9 (2000).

13. M. Hirano, M. Inagaki, Improvement of mechanical and electrical properties of scandia-doped zirconia ceramics by post-sintering with hot isostatic pressing. *J. Am. Ceram. Soc.,* 83 [10] 2619-2621 (2000).

14 Z. Lei, Q. Zhu, Low temperature processing of dense nanocrystalline scandia-doped zirconia (ScSZ) ceramics. *Solid State Ionics*, 176 [37-38] 2791-2797 (2005).

15. J.T.S. Irvine, T. Politova, N. Zakowsky, A. Kruth, S. Tao, R. Travis, O. Attia, "Scandia-Zirconia Electrolytes and Electrodes for SOFCs", Fuel Cell Technologies: State and Perspectives, Eds: N. Sammes, A. Smirnova, O. Vasylyev. Springer, Netherlands, 35-47, 2005.

16. J.T.S. Irvine, J.W.L. Dobson, T. Politova, S. García Martín, A. Shenouda, Co-doping of scandia- zirconia electrolytes for SOFCs, *Faraday Discussions*, 134 41-49 (2007).

17. D.-S. Lee, W.S. Kim, S.H. Choi, J. Kim, H.-W. Lee, J.-H. Lee, Characterization of ZrO_2 co-doped with Sc_2O_3 and CeO_2 electrolyte for application of intermediate temperature SOFCs, *Solid Sta. Ion*., 176 [1-2] 33-39 (2005).

18. Z. Wang, M. Cheng, Z. Bi, Y. Dong, H. Zhang, J. Zhang, Z. Feng, C. Li, Structure and impedance of ZrO_2 doped with Sc_2O_3 and CeO_2, *Mater. Let.* 59 2579-2582 (2005).

19. Waqas Bin Najib, Literature survey of scandia doped zirconia solid electrolyte systems, Risø Nat. Lab. Febr. 2007. Internal Document of project SOFC 600.

20. R.E. Mistler, D.J. Shanfield, R.B. Runk, Ceramic Processing before Firing, Wiley, New York, 411–448, 1978.

21. S. Bhattacharjee, M. K. Paria, H. S. Maiti, Polyvinyl butyral as a dispersant for barium titanate in a non-aqueous suspension, *Journal of Materials Science*, 28 [23] 6490-6495 (1993).

22. M. Chen, T.-L. Wen, Z. Huang, P.-C. Wang, H.-Y. Tu, Z.-Y. Lu, Study on isostatic pressing YSZ membranes fabricated by tape casting, Solid Oxide Fuel Cells (SOFC VI). Proceedings of

the Sixth International Symposium. Eds. S. C. Singhal, M. Dokiya. The Electrochemical Society, Pennington, NJ, 144-149, 1999.

23. M. Rahaman, Ceramic Processing, CRC Press, Boca Raton, FL, p. 337, 2007.

24. T. Chartier, E. Streicher, P. Booch, Phosphate ester as dispersant for the tape casting of alumina, *Ceram. Bull.,* 66 1653–1655 (1987).

25. S. Ramanathan, K. P. Krishnakumar, P. K. De, S. Banerjee, Powder dispersion and aqueous tape casting of YSZ-NiO composite, *Jour. Mater. Sci.*, 39 [10] 3339-3344 (2004).

26. R. Nava, S. Guillemet-Fritsch, J. Aguilar-Garib, E. Reyes, B. Durand, The thickness of $BaTiO_3$ tape castings as function of the slip system, *Journal of Ceramic Processing Research,* 13 [2] 101-104 (2012).

27. A. Jillavenkatesa, L-S. H. Lum; S. Dapkunas, NIST Recommended Practice Guide: Particle Size Characterization. Special Publication 960-1, NIST, Washington, 2001.

28. R.M. Slepian, Preparation of Stabilized Zirconia for Microscopic Examination, *J. Amer. Ceram. Soc.*, 47 [10] 535-536 (1964).

29. U. Taffner, V. Carle, U. Schäfer, Preparation and Microstructural Analysis of High-Performance Ceramics, ASM Handbook, Vol. 9: Metallography and Microstructures, ASM International, Materials Park, OH, 1057-1066, 2004.

30. J. F. Friel, Practical guide to image analysis, ASM International, Materials Park, OH, 188-192, 2000.

31. A. Berger, M. Herwegh., J.-O. Schwarz, B. Putlitz, Quantitative analysis of crystal/grain sizes and their distribution in 2D and 3D, *Journal of Structural Geology*, 33 1751-1763 (2011).

32. F. Yin, A. Sakurai, X. Song, Determination of Spatial Grain Size with the Area-Weighted Grain Area Distribution of the Planar Sections in Polycrystalline Materials, *Metall. Mater. Trans. A*, 37A 3707-3714 (2006).

33. E. Barsoukov, J. R. Macdonald, Impedance Spectroscopy: Theory, Experiment and Applications, 2nd Edition, John Wiley and Sons, Inc., New Jersey, 227-238, 2005.

34. A. Simpatico, W. R. Cannon, M. J. Matthewson, Comparison of Hydraulic-Burst and Ball-on-Ring Tests for Measuring Biaxial Strength, *J. Am. Ceram. Soc.,* 82 [10] 2737–2744 (1999).

35. R.M. Slilaty, M.B. Marques, Electrical conductivity of Yttria Stabilized Zirconia (YSZ) doped with transition metals. *Bol. Soc. Esp. Ceram. y Vid.*, 35 [2] 109-115 (1996).

36. D.Z. Florio, R. Muccillo, Sintering of zirconia-yttria ceramics studied by impedance spectroscopy. *Solid. Sta. Ion.*, 123 301-305 (1999).

37. W. Lai, S.M. Haile, Impedance Spectroscopy as a Tool for Chemical and Electrochemical Analysis of Mixed Conductors: A Case Study of Ceria, *J. Am. Ceram. Soc.*, 88[11] 2979-2997 (2005).

38. W. Preis, J. Waldhäusl, A. Egger, W. Sitte, E. de Carvalho, J.T.S. Irvine, Electrical properties of bulk and grain boundaries of scandia-stabilized zirconia co-doped with yttria and ceria, *Solid State Ionics*, 192 [1] 148–152 (2011).

39. M. Liu, C. R. He, W. G. Wang, J. X. Wang, Synthesis and characterization of 10Sc1CeSZ powders prepared by a solid-liquid method for electrolyte-supported solid oxide fuel cells, *Ceramics International*, 40 [4] 5441-5446 (2014).

40. C.N.S. Kumar, R. Bauri, Enhancing the phase stability and ionic conductivity of scandia stabilized zirconia by rare earth co-doping, *Journal of Physics and Chemistry of Solids*, 75 [5] 642-650 (2014).

41. H.P. Dasari, J. S. Ahn, Kiyong Ahn, S.-Y. Park, J. Hong, H. Kim, K. J. Yoon, J.-W. Son, H.-W. Lee, J.-H. Lee, Synthesis, sintering and conductivity behavior of ceria-doped scandia-stabilized zirconia, *Solid State Ionics,* 263 103-109 (2014).

42. A. Belda, “Estudio del proceso de sinterización de componentes cerámicos para pilas de combustible de óxidos sólidos”. M.S. Thesis, Universitat Jaume I, Castellón, Spain, November 2015.

Figure captions

Fig. 1. Aspect of the best cast sheet obtained using xylene-ethanol as a solvent.

Fig. 2. Thermogravimetric analysis of the best composition using MEK-isopropanol (dry but containing the organic additives).

Fig. 3. DTA diagram of the dry sheet shown in Fig. 2.

Fig. 4. Linear shrinkage versus temperature for the best composition obtained using xylene-ethanol as a solvent.

Fig. 5. Aspect of the sheets heated at 2°C/min up to different maximum temperatures.

Fig. 6. Aspect of the sheets heated at 0.5°C/min up to different maximum temperatures.

Fig. 7. Porosity and mean pore diameter of the sheets obtained at different sintering temperatures and holding times.

Fig. 8. Sintered sheets observed from the surface. Variation of the grain size with sintering temperature and holding time.

Fig. 9. Sintered sheets. Variation of the grain size with sintering temperature and holding time.

Fig. 10. Porosity and mean pore diameter of the pressed specimens at different sintering temperatures and holding times.

Fig. 11. Pressed specimens. Evolution of the average grain size (D_{50}) with sintering temperature and holding time.

Fig. 12. Impedance spectra of pressed samples sintered at different times and temperatures measured at: (a) 300°C and (b) 600°C.

Tables

Table 1. Experimental values of average grain size (D_{50PS}) and total conductivity measured at 600°C (σ_T) of the sintered pressed specimens.

T_S (°C)	t_h (h)	σ_T (mS/cm)	D_{50PS} (μm)
1300	2	12.1	1.52
	4	15.6	1.74
	6	19.0	1.91
1400	2	21.5	2.70
	4	21.6	3.01
	6	21.0	3.30
1500	1	21.5	3.40
	2	20.6	3.80
	4	21.5	4.30
	6	22.0	4.70

Table 2. Porosity (ε), average pore size (d_{50}) and average grain size (D_{50}) of the sintered sheets (subscript S) and sintered pressed specimens (subscript PS).

T_S (°C)	t_h (h)	ε_S (%)	d_{50S}(μm)	D_{50S} (μm)	ε_{PS} (%)	d_{50PS} (μm)	D_{50PS} (μm)
1200	2	6.42	0.34	-	-	-	-
	4	3.20	0.34	-	-	-	-
	6	0.75	0.30	-	-	-	-
1300	2	0.23	0.22	1.32	1.70	0.30	1.52
	4	0.20	0.20	1.49	1.07	0.29	1.74
	6	0.20	0.21	1.76	1.06	0.30	1.91
1400	2	0.35	0.22	2.65	0.99	0.32	2.70
	4	0.17	0.21	3.06	0.96	0.34	3.01
	6	0.10	0.18	3.50	0.88	0.33	3.30
1500	1	-	-	-	0.66	0.33	3.40
	2	0.15	0.24	4.75	0.62	0.33	3.80
	4	0.10	0.28	5.71	0.52	0.34	4.30
	6	0.11	0.26	6.30	0.48	0.35	4.70

Table 1. Experimental values of average grain size (D_{50PS}) and total conductivity measured at 600°C (σ_T) of the sintered pressed specimens.

T_S (°C)	t_h (h)	σ_T (mS/cm)	D_{50PS} (µm)
1300	2	12.1	1.52
	4	15.6	1.74
	6	19.0	1.91
1400	2	21.5	2.70
	4	21.6	3.01
	6	21.0	3.30
1500	1	21.5	3.40
	2	20.6	3.80
	4	21.5	4.30
	6	22.0	4.70

Table 2. Porosity (ε), average pore size (d_{50}) and average grain size (D_{50}) of the sintered sheets (subscript S) and sintered pressed specimens (subscript PS).

T_S (°C)	t_h (h)	ε_S (%)	d_{50S}(µm)	D_{50S} (µm)	ε_{PS} (%)	d_{50PS} (µm)	D_{50PS} (µm)
1200	2	6.42	0.34	-	-	-	-
	4	3.20	0.34	-	-	-	-
	6	0.75	0.30	-	-	-	-
1300	2	0.23	0.22	1.32	1.70	0.30	1.52
	4	0.20	0.20	1.49	1.07	0.29	1.74
	6	0.20	0.21	1.76	1.06	0.30	1.91
1400	2	0.35	0.22	2.65	0.99	0.32	2.70
	4	0.17	0.21	3.06	0.96	0.34	3.01
	6	0.10	0.18	3.50	0.88	0.33	3.30
1500	1	-	-	-	0.66	0.33	3.40
	2	0.15	0.24	4.75	0.62	0.33	3.80
	4	0.10	0.28	5.71	0.52	0.34	4.30
	6	0.11	0.26	6.30	0.48	0.35	4.70

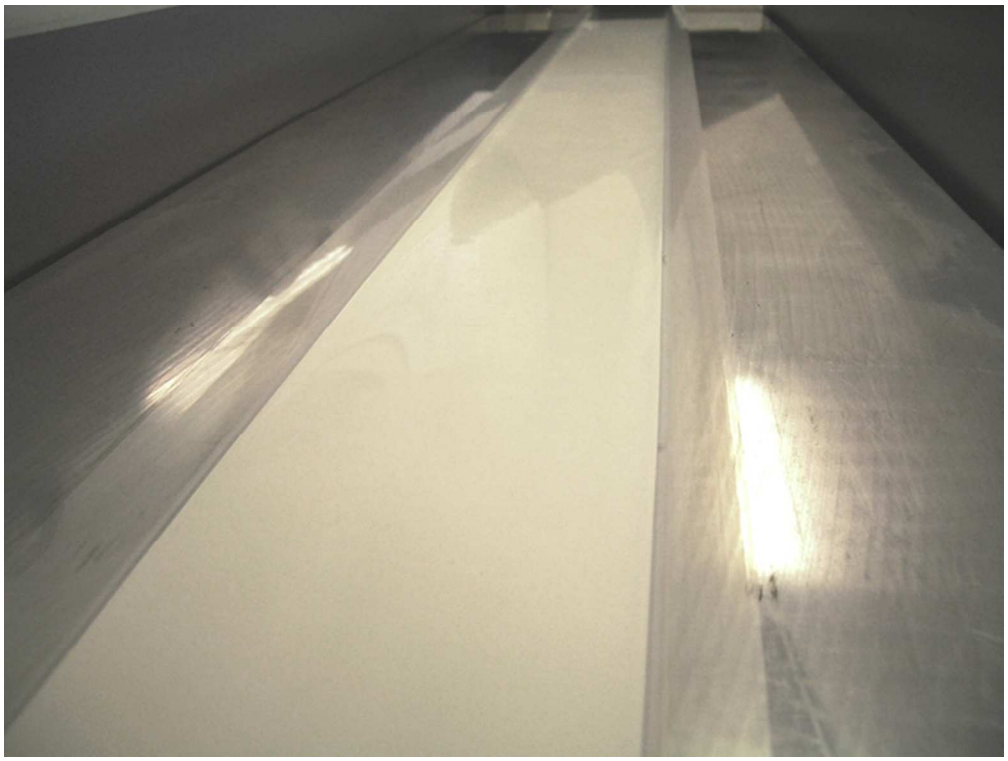

Caption : Fig. 1. Aspect of the best cast sheet obtained using xylene-ethanol as a solvent.

60x45mm (300 x 300 DPI)

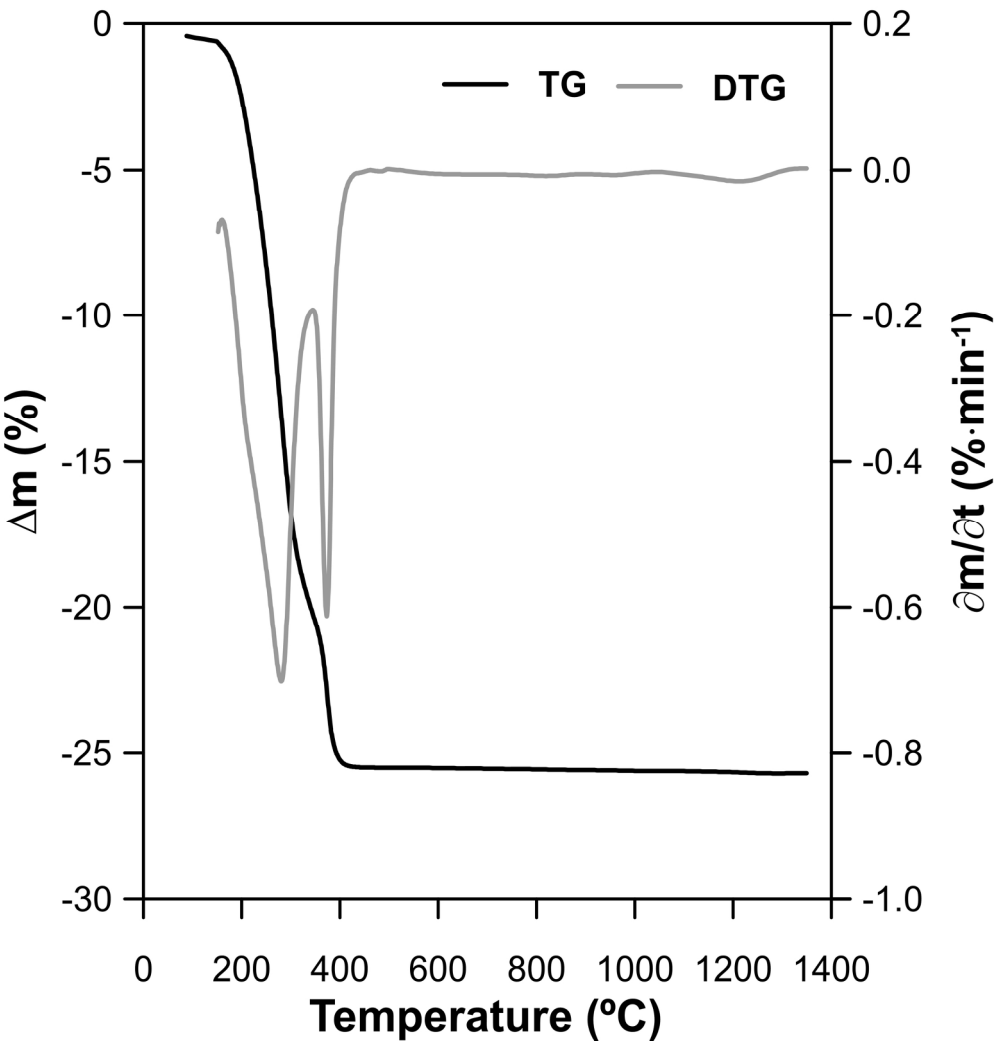

Fig. 2. Thermogravimetric analysis of the best composition using MEK-isopropanol (dry but containing the organic additives).

93x96mm (600 x 600 DPI)

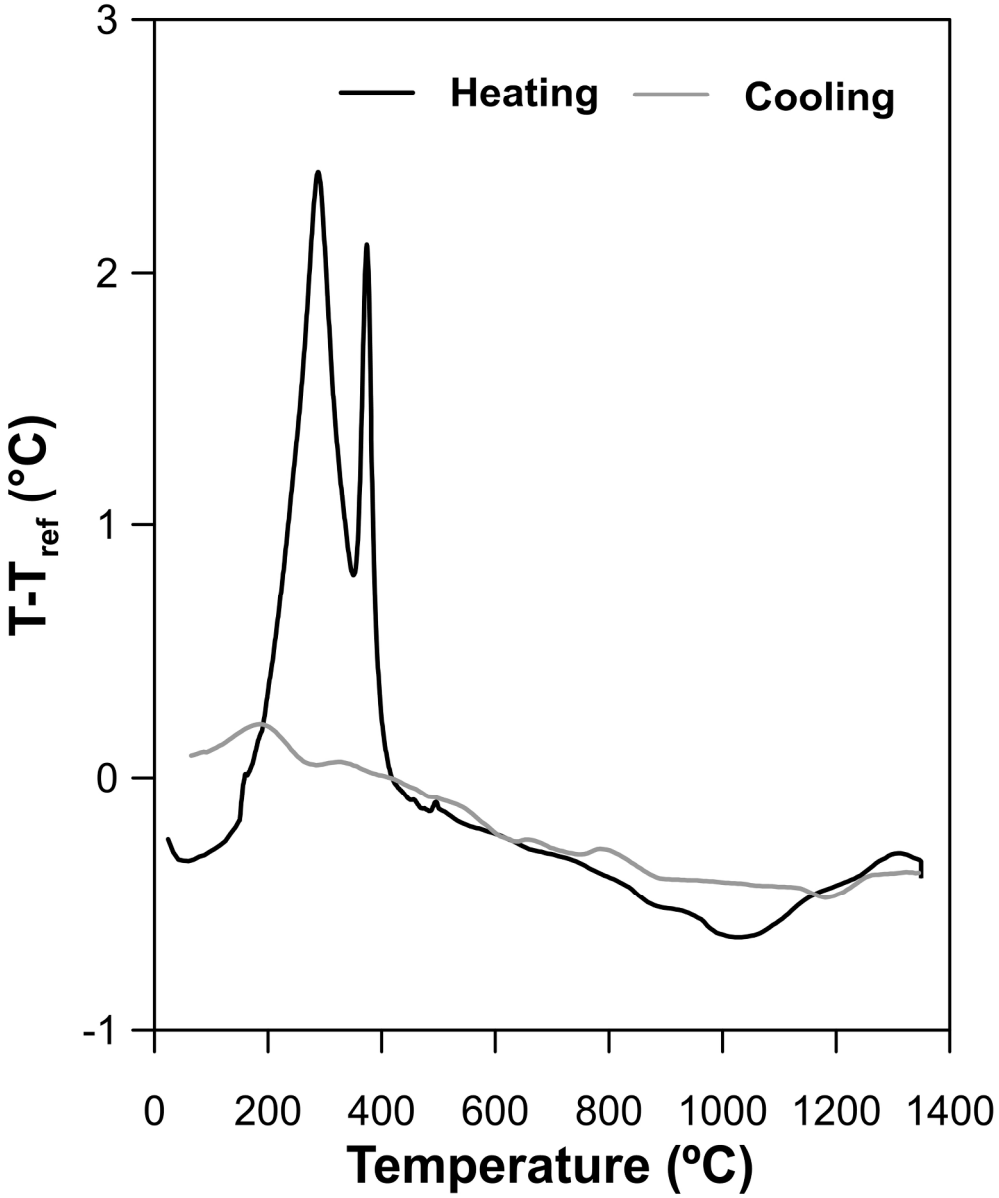

Fig. 3. DTA diagram of the dry sheet shown in Fig. 2.

107x128mm (600 x 600 DPI)

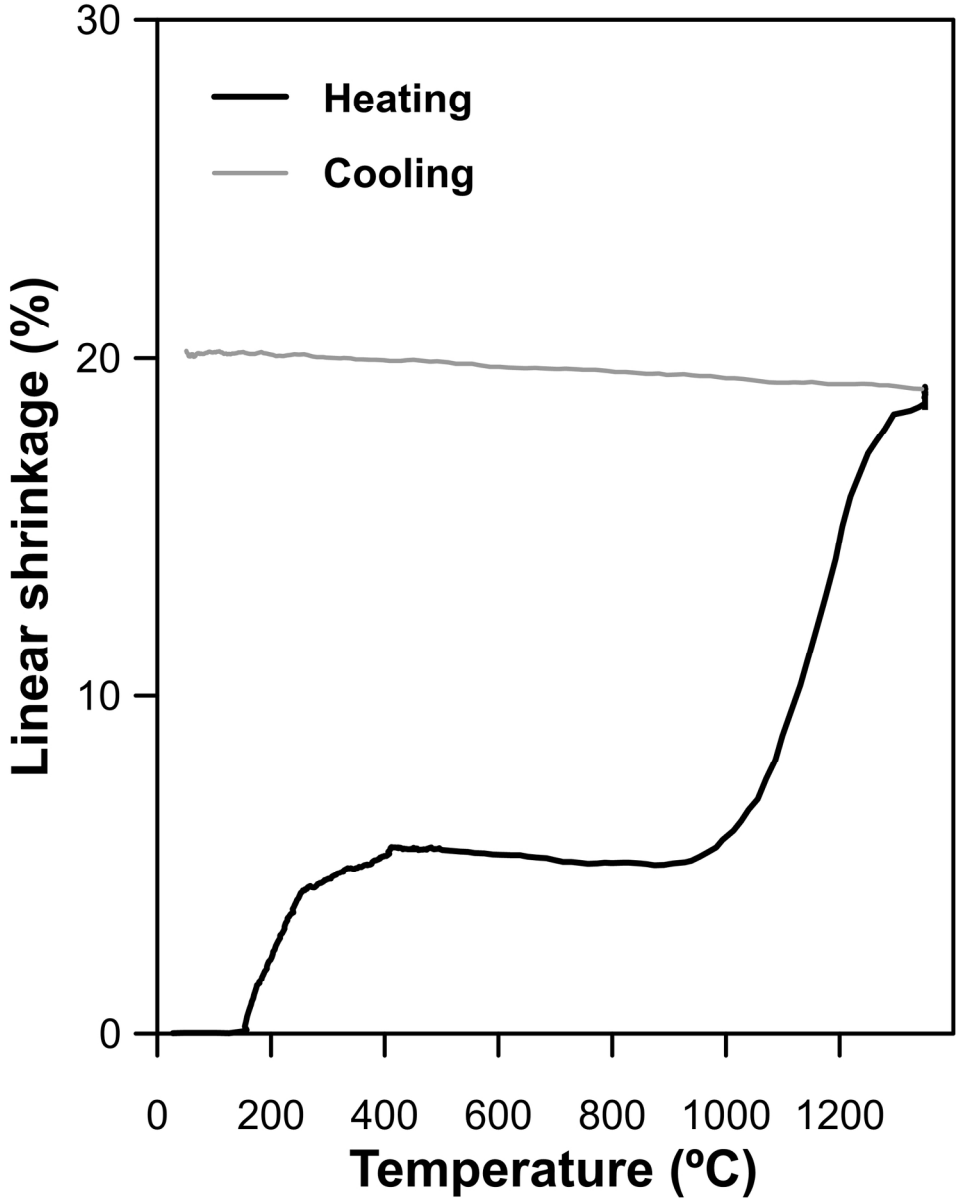

Fig. 4. Linear shrinkage versus temperature for the best composition obtained using xylene-ethanol as a solvent.

82x103mm (600 x 600 DPI)

Fig. 5. Aspect of the sheets heated at 2°C/min up to different maximum temperatures.

90x119mm (300 x 300 DPI)

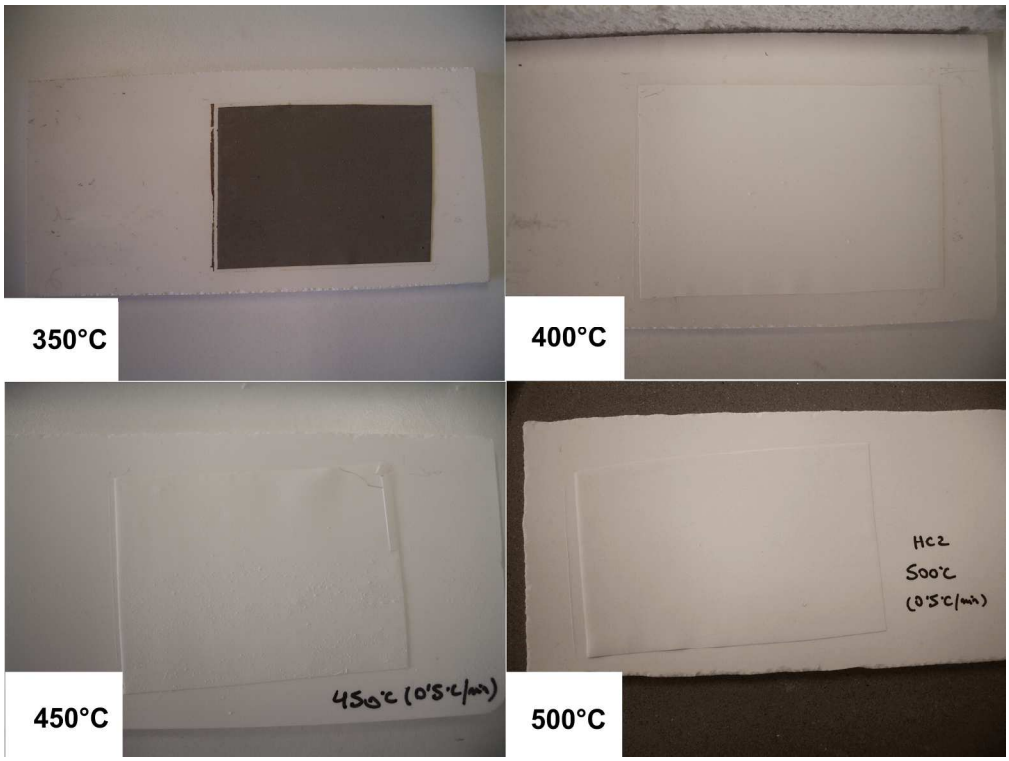

Fig. 6. Aspect of the sheets heated at 0.5°C/min up to different maximum temperatures.

199x150mm (300 x 300 DPI)

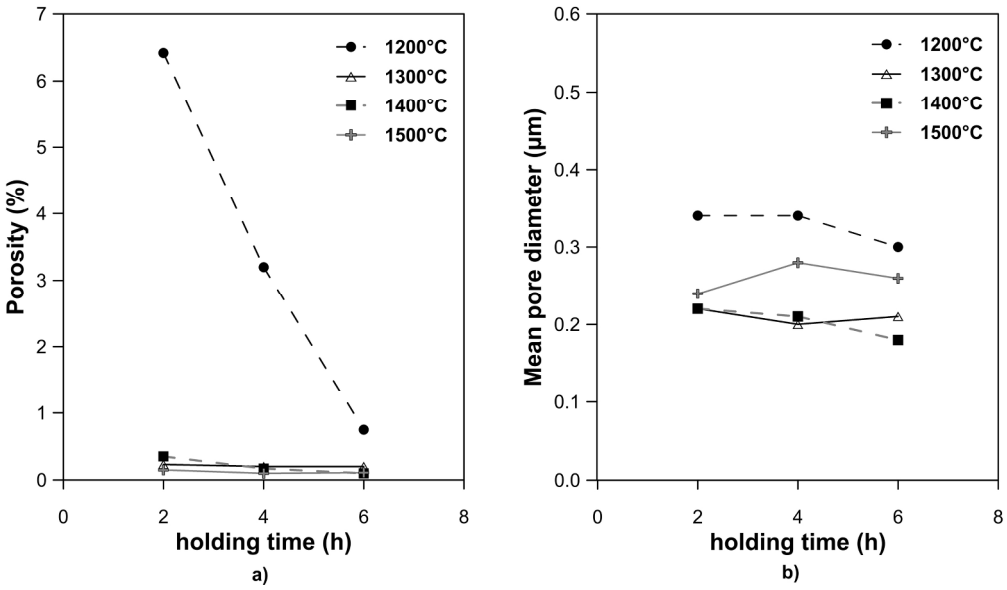

Fig. 7. Porosity and mean pore diameter of the sheets obtained at different sintering temperatures and holding times.

110x64mm (600 x 600 DPI)

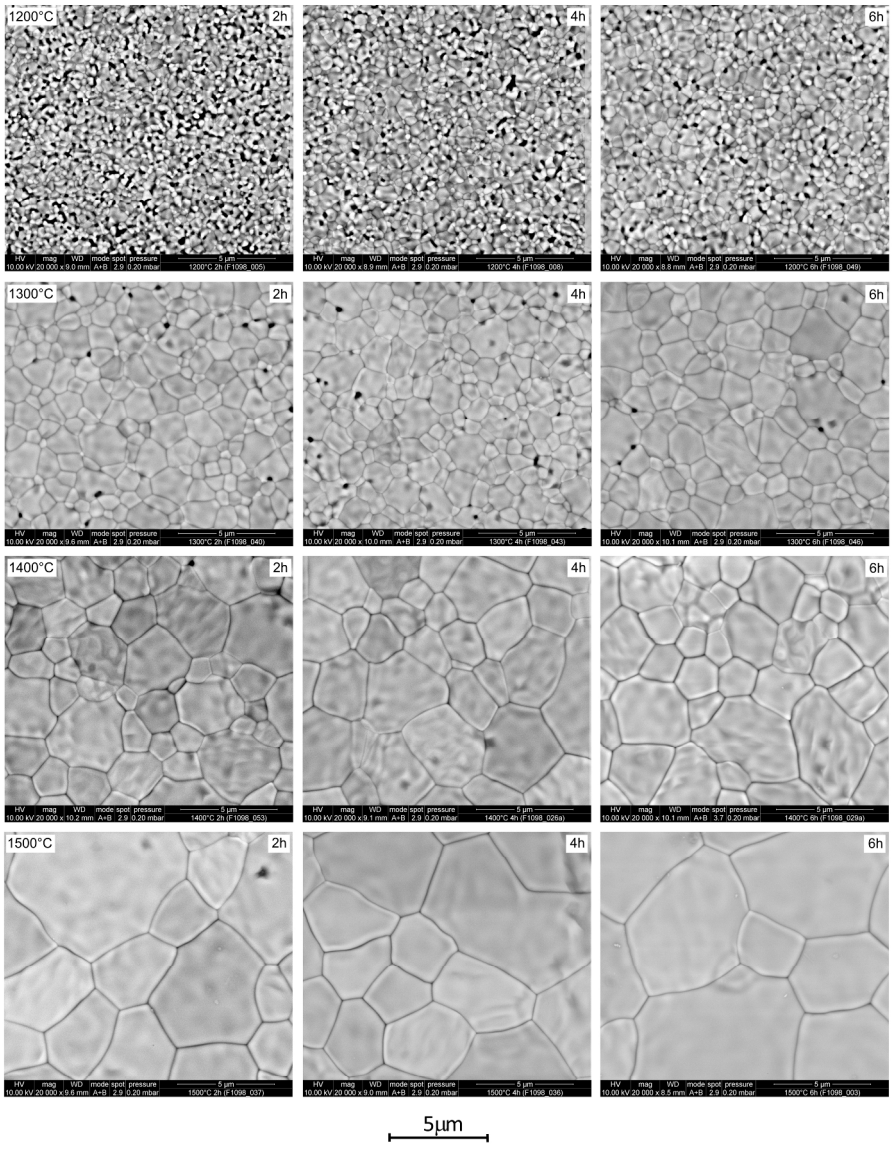

Fig. 8. Surface of the sintered sheets. Variation of the grain size with sintering temperature and holding time.

253x337mm (300 x 300 DPI)

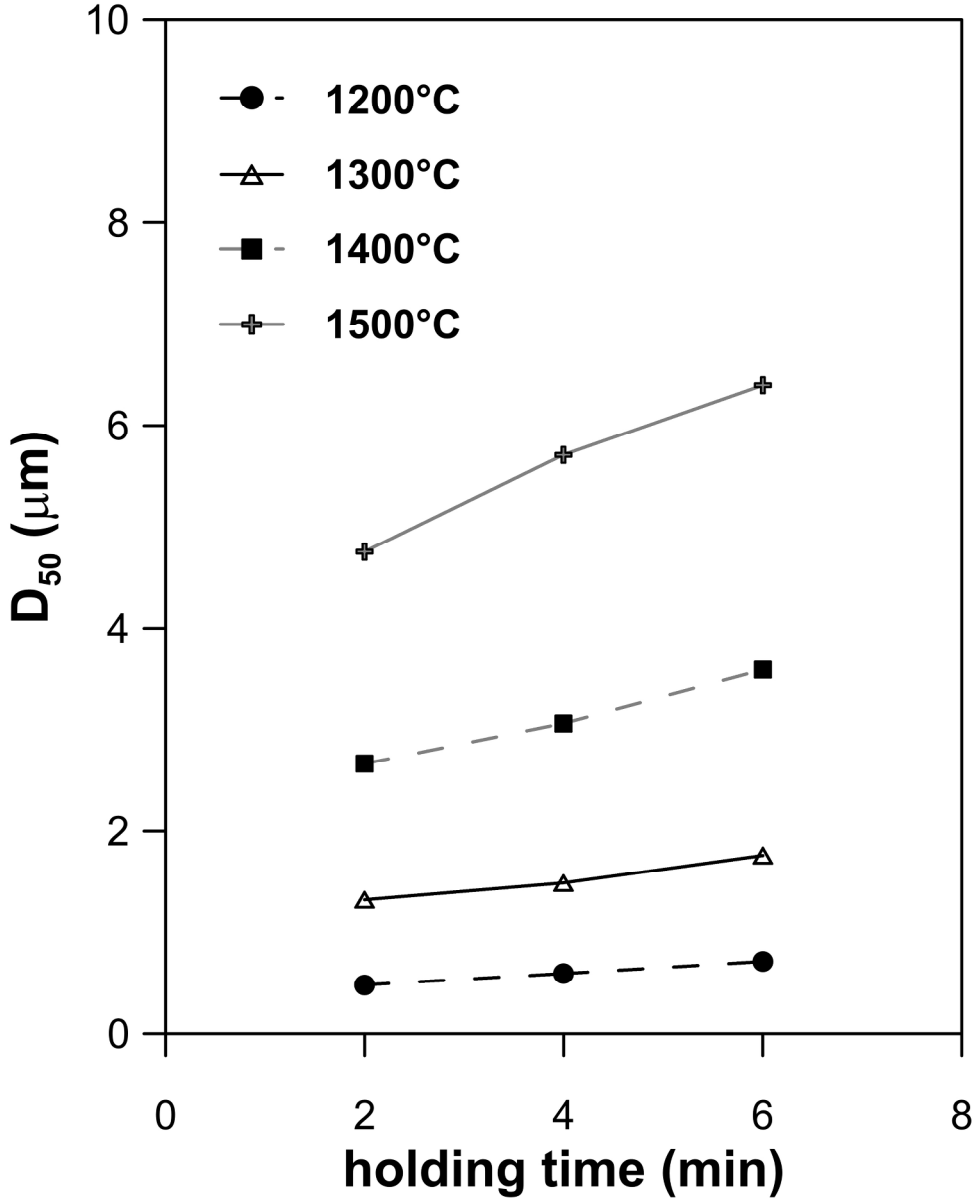

Fig. 9. Sintered sheets. Variation of the grain size with sintering temperature and holding time.

110x135mm (600 x 600 DPI)

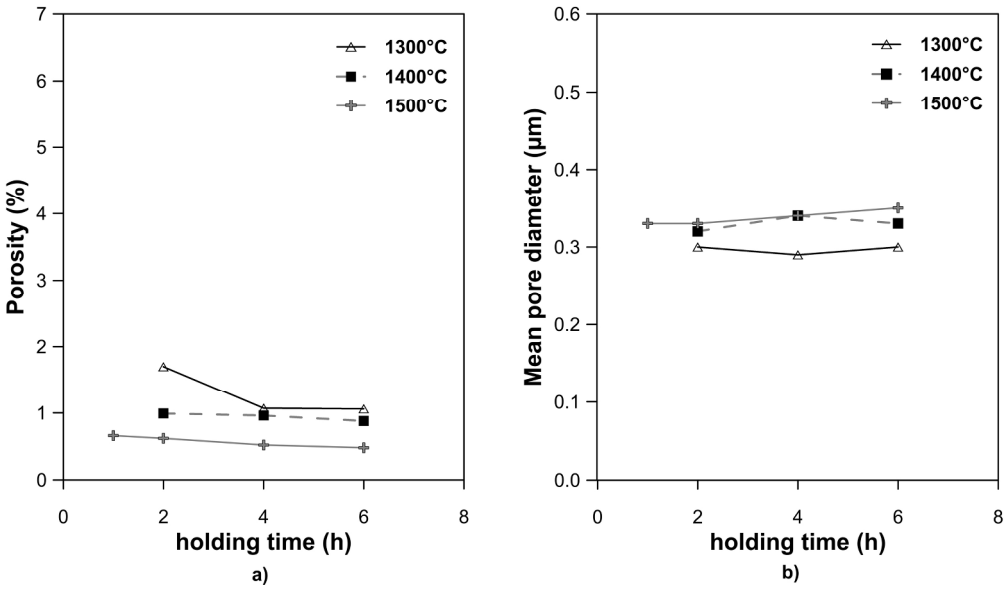

Fig. 10. Porosity and mean pore diameter of the pressed specimens at different sintering temperatures and holding times.

110x64mm (600 x 600 DPI)

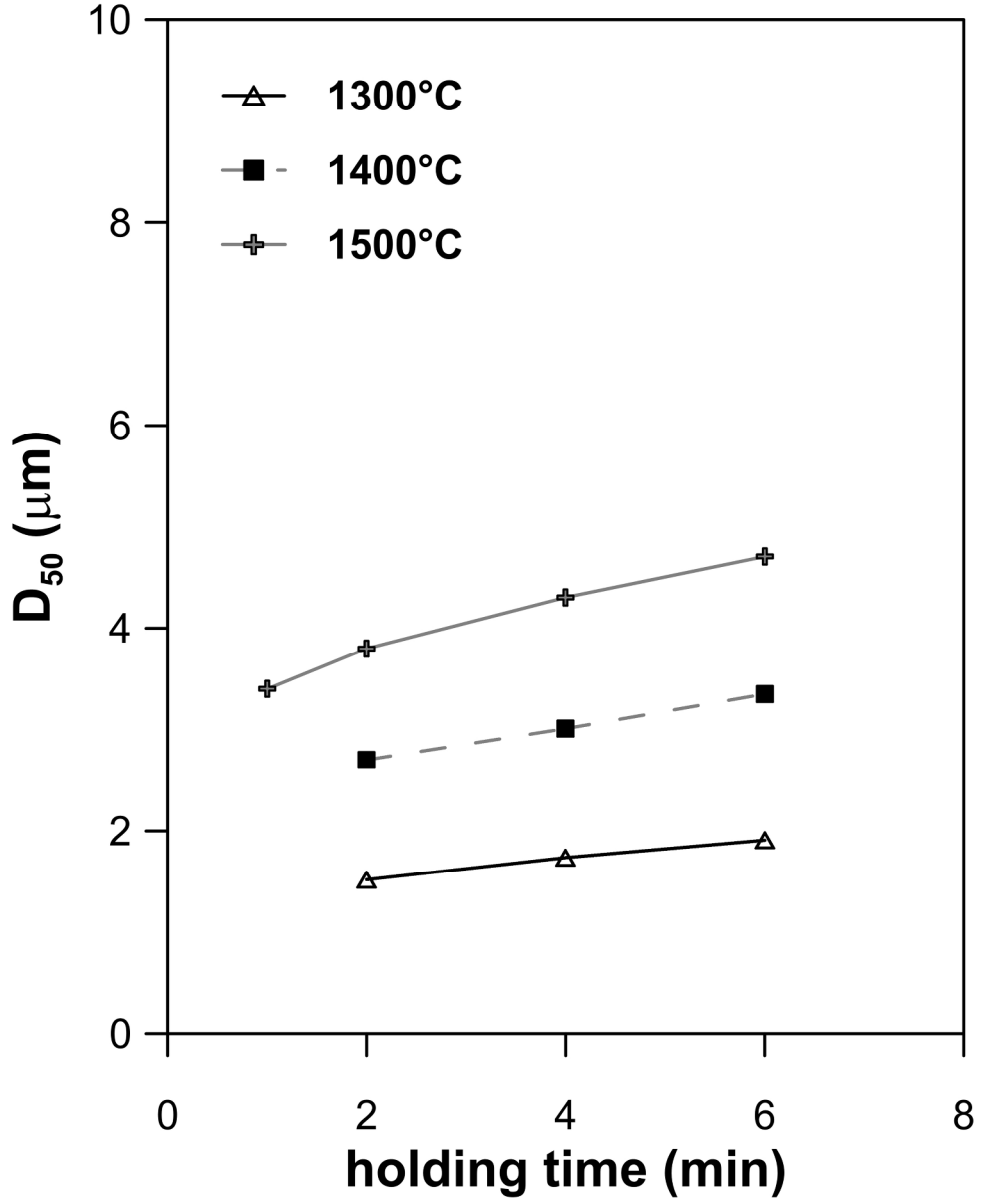

Fig. 11. Pressed specimens. Evolution of the average grain size (D_{50}) with sintering temperature and holding time.

110x135mm (600 x 600 DPI)

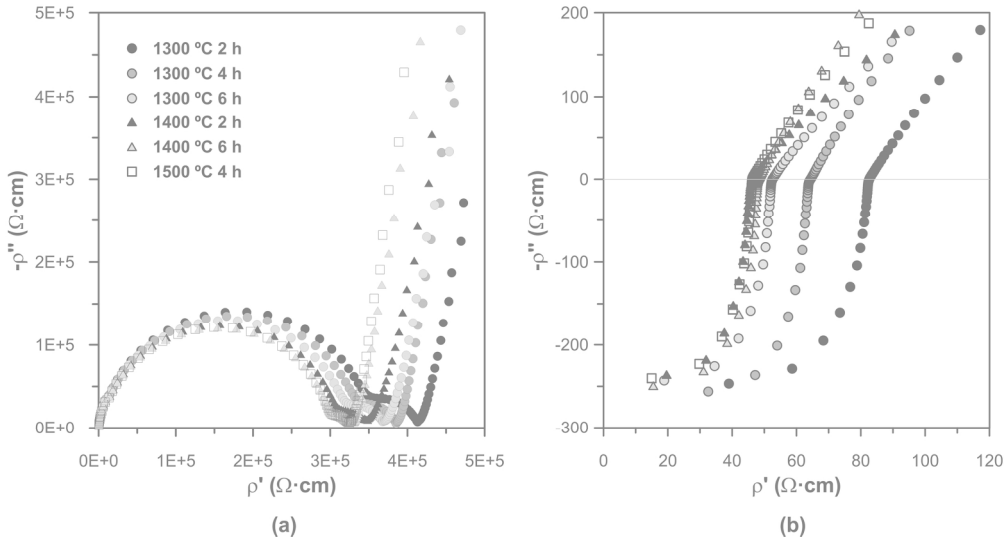

Fig. 12. Impedance spectra of the pressed samples sintered at different times and temperatures, measured at: (a) 300°C and (b) 600°C.

89x47mm (600 x 600 DPI)